

Quasinormal modes of scalar and Dirac perturbations of Bardeen de-Sitter black holes

Wadbor Wahlang^{*}

Piyush A. Jeena[†]

S. Chakrabarti[‡]

Department of Physics

Indian Institute of Technology Guwahati
Guwahati-781039, India

Abstract

We compute the quasi-normal (QN) frequencies for the regular Bardeen de Sitter (BdS) black hole due to massless and massive scalar field perturbations as well as the massless Dirac perturbations. We analyze the behaviour of both real and imaginary parts of quasinormal frequencies by varying the black hole parameters.

1 Introduction

In the study of physics, the stability criteria of a system or configuration is one of the main interesting aspects. Unstable system or configurations are generally not realizable in nature and they are generally an intermediate stage in the dynamical evolution of a system. A black hole system in general relativity can also be put in the above mentioned category: the question one asks there is whether a black hole which is stable under some perturbation, i.e. if we perturb the black hole from outside, whether it comes back to its original state after some time or whether the perturbation grows unbound making the black hole unstable.

The study of black hole perturbations remains an extremely intriguing topic which has enormous effect on various important properties of a black hole [1, 2, 3, 4]. In general, the dynamical evolution of perturbations of a black hole background can be classified into three stages, the first of which consists of an initial outburst of wave, depending completely on the initial perturbing field, the second stage consists of damped oscillations, known in the literature as the quasinormal modes (QNM) whose frequency turns out to be a complex number, the real part representing the oscillation frequency and the imaginary part representing damping. QN frequencies completely depend on the background and not on the field which is causing the perturbation and thereby giving immense importance to these modes which are used to determine the black hole parameters (mass, charge and angular momentum). The third is a power law tail behaviour at very late times. The equations governing the black hole perturbations in most of the cases can be cast into a Schrödinger like wave equation. The QNMs are solutions to the wave equation with complex frequencies with a boundary condition which are completely ingoing at the horizon and purely outgoing at asymptotic infinity. With the first ever detection of the gravitational wave [5] the interest in studying black hole perturbations has gained another peak. Apart from the fact that the QN frequencies contain important information about the black hole parameters, they were also found to be important from the point of view of AdS/CFT correspondence. It has been found that QNMs in AdS space time appear naturally in the description of the dual conformal field theory on

^{*}Email: wadbor@iitg.ernet.in

[†]Email: p.jeena@iitg.ernet.in

[‡]Email: sayan.chakrabarti@iitg.ernet.in

the boundary [6, 7], thereby directing the study of QNMs towards AdS black holes [8, 9]. Although the QNMs are classical in origin, they have been shown to provide glimpses to quantum nature of black holes [10, 11, 12]. However, in the present work we will be focussing on the second of the above three stages of evolution of black hole perturbation in a regular black hole background in asymptotically de Sitter space time.

The importance of studying black holes in de Sitter space lies in the fact that our universe looks like asymptotically de Sitter at very early and late times. Recent observational data also indicates that our universe is going through a phase of accelerated expansion [13, 14, 15], thereby providing the existence of a positive cosmological constant. In general de Sitter space turns out to be a maximally symmetric solution to the vacuum Einstein equations with a positive cosmological constant. Just like the AdS/CFT correspondence, a holographic dS/CFT duality exists between gravity in de Sitter space and conformal field theory on the boundary in one less dimension [16, 17, 18]. Coming back to the perturbations and stability of black holes in de Sitter space, there have been a lot of work [19]-[28] on quasinormal modes of scalar, electromagnetic, gravitational, Dirac perturbations, decay of charged fields, asymptotic quasinormal modes and signature of quantum gravity etc. On another front, it is well known that general relativity is plagued with the appearance of singularities. The problem of avoiding the singularities in general relativity therefore is one of the most fundamental ones and it is a very old problem. In this regard, “regular black hole” solutions play a central role. When a black hole does not have a space time singularity at the origin, it is termed as a “regular black hole” in the literature. The first solution of such regular black holes with non-singular geometry satisfying the weak energy condition was obtained by Bardeen [29], which is now known as the Bardeen black hole. However, the solution Bardeen proposed lacked physical motivation because the solution was not a vacuum solution, rather gravity was modified by introducing some form of matter and thereby introducing an energy momentum tensor in the Einstein’s equation. The introduction of the energy momentum tensor was done in an *ad hoc* manner. Much later, Ayón-Beato and García [30] showed the energy momentum tensor to be the gravitational field of some magnetic monopole arising out of a specific form of non-linear electrodynamics. Subsequently, many other solutions [31]-[35], motivating the avoidance of singularity was proposed in the literature. There were many works published regarding such regular black holes: stability properties [36], QNMs [37, 38], thermodynamics [39] and geodesic structure [40] of regular black holes to mention a few. Very recently Fernando [41] has proposed a de Sitter branch for the regular Bardeen black hole and calculated the grey body factor for such a black hole. In this paper, we will be discussing the QNMs of the Bardeen de Sitter (henceforth BdS) black hole due to scalar (both massless and massive) and Dirac perturbations. Although study of scalar field perturbations in a black hole background and its corresponding QNMs is not new, the Dirac field perturbations on the other hand are relatively less studied. Therefore, apart from the scalar perturbations, it will also be interesting to study the Dirac perturbations in the regular black hole backgrounds in de Sitter space.

The plan of the paper is as follows: in the next section we briefly discuss the BdS black hole. In section 3 we present a brief discussion of WKB method along with a study of the scalar QNMs of the BdS black holes. Section 4 deals with the Dirac quasinormal modes of the BdS black hole. Finally, in section 5 we conclude the paper with a brief discussion on future directions.

2 A discussion on BdS black hole

In this section we will briefly discuss about the Bardeen de Sitter (BdS) black hole following the works of Fernando [41]. The author of this paper modified the works of [30] to incorporate a positive cosmological constant in the action:

$$S = \int d^4x \sqrt{-g} \left(\frac{R - 2\Lambda}{16\pi} - \frac{1}{4\pi} \mathcal{L}(F) \right), \quad (1)$$

where R is the Ricci Scalar and $\mathcal{L}(F)$ is function of the field strength tensor of the non-linear electrodynamics $F_{\mu\nu} = 2(\nabla_\mu A_\nu - \nabla_\nu A_\mu)$ and its form is given by

$$\mathcal{L}(F) = \frac{3}{2\alpha g^2} \left(\frac{\sqrt{2g^2 F}}{1 + \sqrt{2g^2 F}} \right)^{5/2}. \quad (2)$$

In the above, the parameter α is related to the magnetic charge and the mass of the black hole in the following manner: $\alpha = \frac{g}{2M}$. If one derives the equations of motion from the above action(1), then following equations will be arrived at

$$G_{\mu\nu} + \Lambda g_{\mu\nu} = 2 \left(\frac{\partial \mathcal{L}(F)}{\partial F} F_{\mu\lambda} F_{\nu}^{\lambda} - g_{\mu\nu} \mathcal{L}(F) \right) \quad (3)$$

$$\nabla_{\mu} \left(\frac{\partial \mathcal{L}(F)}{\partial F} F^{\nu\mu} \right) = 0 \quad (4)$$

$$\nabla_{\mu} (*F^{\nu\mu}) = 0 \quad (5)$$

It was shown in [41] that a static spherically symmetric solution for the above set of equations exist:

$$ds^2 = -f(r)dt^2 + f(r)^{-1}dr^2 + r^2(d\theta^2 + \sin^2\theta d\phi^2) \quad (6)$$

with $f(r)$ being given

$$f(r) = 1 - \frac{2Mr^2}{(r^2 + g^2)^{3/2}} - \frac{\Lambda r^2}{3}. \quad (7)$$

The solution of $f(r) = 0$ gives the horizon and in the particular case of BdS black hole there may be three real roots implying three horizons: the black hole inner and outer horizons along with the cosmological horizon. There lies the possibility of getting either one real root corresponding to cosmological horizon only for a set of parameters of this theory or a possibility of getting degenerate roots corresponding to a merger of the inner and outer black hole horizons for a range of parameters M, g and Λ . Structurally the BdS black hole is similar to the Reissner-Nordström-de Sitter (RNds) or Born-Infeld de Sitter (BIdS) black holes which also admits a possibility of three distinct horizons as well as a single or degenerate horizons. However, it was shown in [41] that the event horizon is larger in case of RNds black hole compared to a BdS one. The interesting nature of BdS geometry is its non-singular structure everywhere. It can be checked by direct calculation that all the scalar curvatures $R, R_{\mu\nu}R^{\mu\nu}, R_{\mu\nu\lambda\sigma}R^{\mu\nu\lambda\sigma}$ are finite everywhere except the electromagnetic field invariant F which is singular at $r = 0$ [41].

3 QNMs of massless and massive scalar perturbations in BdS black hole

In this section we will consider the massless and massive scalar field perturbations of the BdS black hole geometry to study the behaviour of the QNMs in BdS background with the given black hole parameters.

3.1 Massless scalar field perturbation

As discussed in Section 2, BdS background metric is given by Eqns. (6) and (7). The Klein-Gordon equation for a massless scalar field Φ is

$$\nabla^2 \Phi = 0, \quad (8)$$

which explicitly takes the form

$$\frac{1}{\sqrt{-g}} \partial_{\mu} \left(\sqrt{-g} g^{\mu\nu} \partial_{\nu} \Phi \right) = 0 \quad (9)$$

As usual, we introduce the ansatz for Φ as,

$$\Phi = e^{-i\omega t} Y_{\ell,m}(\theta, \phi) \frac{U(r)}{r}. \quad (10)$$

With the above ansatz we have the standard Schrödinger-like wave equation for the perturbation of the BdS metric by a scalar field given by

$$\frac{d^2 U(r)}{dr_*^2} + (\omega^2 - V_{\text{scalar}}(r_*)) U(r) = 0 \quad (11)$$

where, $V_{\text{scalar}}(r) = f(r) \left(\frac{\ell(\ell+1)}{r^2} + \frac{f'(r)}{r} \right)$. The coordinate r_* is the standard tortoise coordinate

related to radial coordinate r as $dr_* = \frac{dr}{f(r)}$. The advantage of using the tortoise coordinate lies in the fact that the range of the coordinate now extends between $-\infty$ to ∞ , whereas in the old radial coordinate r , the physically accessible region lies between the black hole and cosmological horizon. Note also that the potential $V_{\text{scalar}}(r) \rightarrow 0$ as $r_* \rightarrow \pm\infty$.

It can be easily seen by plotting the scalar field potential against the radial coordinate for various values of the multipole number ℓ that the $\ell = 0$ mode has a distinct local minimum between the black hole outer horizon and the cosmological horizon (see Fig. 1), which was also pointed out in [41]. For this reason, the method used in this paper to evaluate the QNMs for the BdS black hole, namely the WKB approach is not a valid one to evaluate QNMs for $\ell = 0$ modes. Therefore, from now on, we will only talk about $\ell \neq 0$ modes for the massless scalar QNMs of BdS black hole.

As already stated, we will solve the wave equation for complex QN frequencies semi-analytically, using the sixth order WKB method developed in [47]. It has been shown extensively in literature that WKB method works extremely well for determining QN frequencies. The sixth order WKB method is more accurate than the third order method and the former in fact gives results practically coinciding with those obtained from full numerical integration of the wave equation [47] for low overtones, i.e. for modes with small imaginary parts, and for all multipole numbers $\ell \geq 1$. The sixth order formula for a general black hole potential $V(r)$ is mentioned below

$$\frac{i(\omega^2 - V(r_0))}{\sqrt{-2V''(r_0)}} - \Lambda_2 - \Lambda_3 - \Lambda_4 - \Lambda_5 - \Lambda_6 = n + \frac{1}{2} \quad (12)$$

where $V(r_0)$ is peak value of $V(r)$, $V''(r_0) = \frac{d^2V}{dr^2}|_{r=r_0}$, r_0 is the value of the radial coordinate corresponding to the maximum of the potential $V(r)$ and n is the overtone number. QN frequencies ω would be of the form $\omega = \omega_R + i\omega_I$. In eqn.[12], Λ_2 and Λ_3 are given by [46]

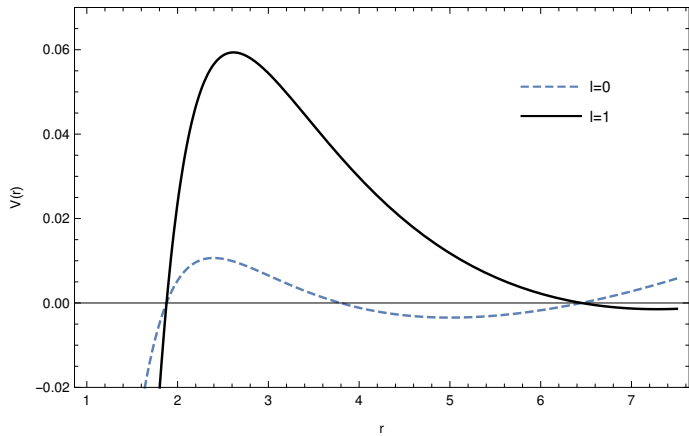


Figure 1: Variation of effective potential $V_{\text{scalar}}(r)$ vs r for $\ell = 0, 1$ with $M = 1$, $g = 0.55$, $\Lambda = 0.05$. Note the negative minimum between the cosmological and black hole horizon in the $\ell = 0$ plot.

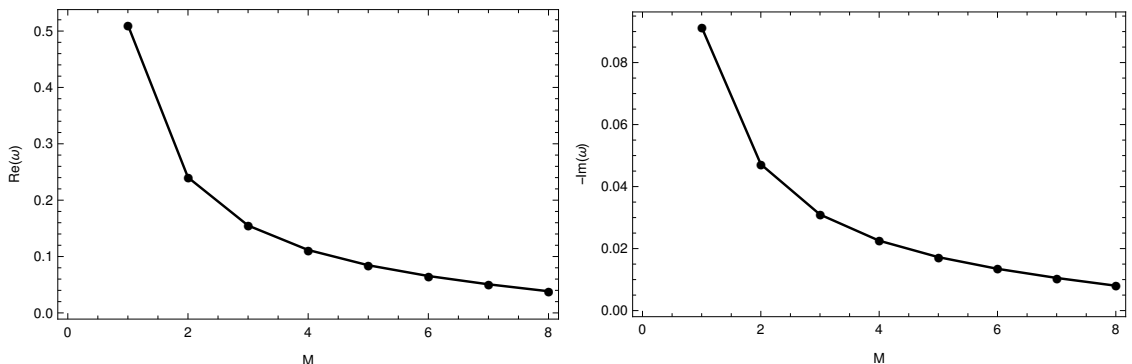


Figure 2: $\text{Re } \omega$ and $\text{Im } \omega$ vs black hole mass M

$$\Lambda_2 = \frac{1}{\sqrt{2V''(r_0)}} \left[\frac{1}{8} \left(\frac{V_0^{(4)}}{V''(r_0)} \right) (b^2 + \frac{1}{4}) - \frac{1}{288} \left(\frac{V_0^{(3)}}{V''(r_0)} \right)^2 (7 + 60b^2) \right] \quad (13)$$

$$\begin{aligned} \Lambda_3 = & \frac{(n + \frac{1}{2})}{2V''(r_0)} \left[\frac{5}{6912} \left(\frac{V_0^{(3)}}{V''(r_0)} \right)^4 (77 + 188b^2) - \frac{1}{384} \left(\frac{(V_0^{(3)})^2 V_0^{(4)}}{(V''(r_0))^3} \right) (51 + 100b^2) \right. \\ & + \frac{(n + \frac{1}{2})}{2V''(r_0)} \left[\frac{1}{2304} \left(\frac{V_0^{(4)}}{V''(r_0)} \right)^2 (67 + 68b^2) + \frac{1}{288} \left(\frac{V_0^{(3)} V_0^{(5)}}{(V''(r_0))^2} \right) (19 + 28b^2) \right. \\ & \left. \left. - \frac{1}{288} \left(\frac{V_0^{(6)}}{V''(r_0)} \right) (5 + 4b^2) \right] \right]. \end{aligned} \quad (14)$$

In the above expression $b = n + \frac{1}{2}$, $V_0^{(n)} = d^n V / dr_*^n$ at $r = r_0$ and Λ_4 , Λ_5 and Λ_6 can be found in the Appendix of [47]. The above method also works extremely well in the eikonal limit of large ℓ corresponding to large quality factor, which will also be discussed in the paper. Using Eqn (12), we computed the QNMs and in figure 2 we plotted $\text{Re } \omega$ and magnitude of $\text{Im } \omega$ vs black hole mass. Both $\text{Re } \omega$ and $\text{Im } \omega$ decreases when mass M is increased. In Table 1, we list the values of the QN frequencies obtained by using third order and sixth order WKB approach for the parameter range $\Lambda = 0.007$ and $g = 0.57$. The data from the table suggests that the value of the real part of the frequency shows a steady increase over its third order outcome but on the other hand, the negative imaginary part obtained using sixth order WKB method shows a steady decline when compared to the third order result. In figures (3) & (4) we plot the behaviour of low lying QN

Multipole number	Overtone number	3rd order WKB	6th order WKB
$\ell=1$	$n=0$	0.300446 -0.089967i	0.302242 -0.090150i
	$n=1$	0.278912 -0.278097i	0.282993 -0.277074i
$\ell=2$	$n=0$	0.499385 -0.088861i	0.499841 -0.088903i
	$n=1$	0.485040 -0.269800i	0.486281 -0.269658i
	$n=2$	0.461291 -0.456456i	0.462177 -0.458553i
$\ell=3$	$n=0$	0.698242 -0.088552i	0.698417 -0.088563i
	$n=1$	0.687778 -0.267316i	0.688277 -0.267273i
	$n=2$	0.669085 -0.449812i	0.669173 -0.450547i
	$n=3$	0.644523 -0.635942i	0.643394 -0.640730i
$\ell=4$	$n=0$	0.897184 -0.088421i	0.897268 -0.088426i
	$n=1$	0.888985 -0.266272i	0.889230 -0.266255i
	$n=2$	0.873746 -0.446645i	0.873717 -0.446952i
	$n=3$	0.853024 -0.629992i	0.851862 -0.632179i
	$n=4$	0.828001 -0.815925i	0.825285 -0.823178i
$\ell=5$	$n=0$	1.09619 -0.088354i	1.09624 -0.088356i
	$n=1$	1.08946 -0.265738i	1.08960 -0.265730i
	$n=2$	1.07666 -0.444914i	1.07663 -0.445061i
	$n=3$	1.05883 -0.626438i	1.05796 -0.627545i
	$n=4$	1.03691 -0.810304i	1.03452 -0.814191i
	$n=5$	1.01159 -0.996158i	1.00748 -1.005740i

Table 1: The QN frequencies due to massless scalar perturbation for multipole number ℓ ranging between 1 to 5 with $\Lambda = 0.007$, and $g = 0.57$.

frequencies vs Λ and g for different ℓ . Both the plots reveals that $\text{Re } \omega$ and $\text{Im } \omega$ decreases with increasing Λ . Real part of frequencies still increasing steadily with g increased and Imaginary part decreases in magnitude. We have also computed the QN frequencies for larger multipole number ℓ with overtone $n = 0$ only. We plot for ℓ ranging between 1 to 40 while we have fixed the values of $\Lambda = 0.001$, $g = 0.55$ and $n = 0$. $\text{Re}(\omega)$ increases linearly with ℓ [42] while magnitude of $\text{Im}(\omega)$ first decreases and remains constant for larger ℓ .

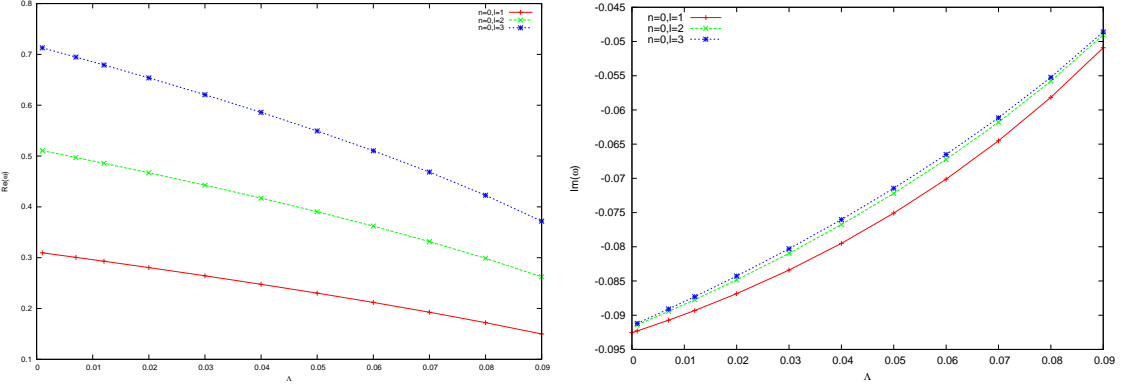


Figure 3: $\text{Re } \omega$ and $\text{Im } \omega$ vs Λ for $g = 0.55$ and $M = 1$

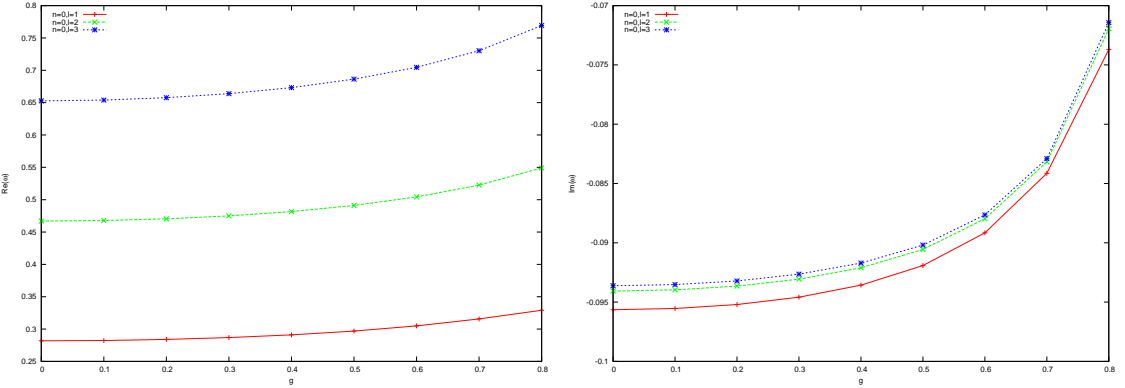


Figure 4: $\text{Re } \omega$ and $\text{Im } \omega$ vs g for $\Lambda = 0.007$ and $M = 1$

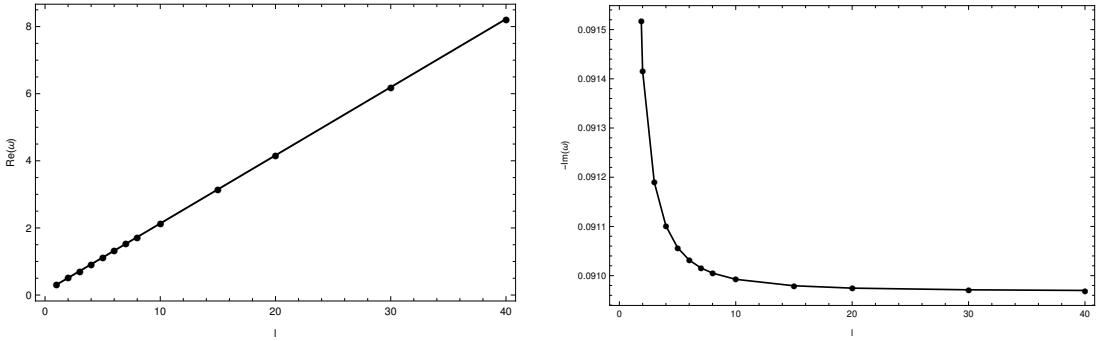


Figure 5: Variation of $\text{Re } \omega$ and $\text{Im } \omega$ with multipole number ℓ . Here $M=1$, $g=0.55$, $\Lambda = 0.001$.

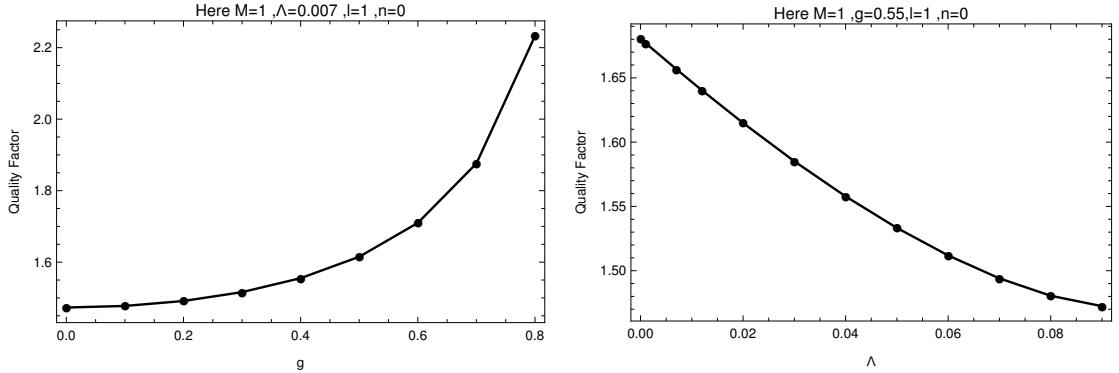


Figure 6: Q-factor vs parameters Λ and g .

To examine the field oscillations, we will define the Quality Factor(Q.F) as

$$Q.F = \frac{Re(\omega)}{2|Im(\omega)|} \quad (15)$$

We plotted the Q.F versus the parameters Λ and g in figure 6. Quality Factor increases with increasing g and decreases with an increase in Λ . Thus, Q.F implies that oscillations will be more with larger magnetic charge g and decay faster for small Λ .

It is worth mentioning here that by computing the Lyapunov exponent (the inverse of the instability timescale associated with the geodesic motion), one can show that, in the eikonal limit, QNMs of black holes in any dimensions are determined by the parameters of the circular null geodesics [43]. This is a very strong result and is independent of the field equations. The only assumption goes into the calculation is the fact that the black hole spacetime is static, spherically symmetric and asymptotically flat. However a non-trivial example of non-asymptotically flat near extremal Schwarzschild de Sitter black hole space time was also discussed in this context. The same argument can be applied in case of BdS black holes too in the limit of near extremal Nariai or cold black holes where either the black hole horizon and the cosmological horizon merges or the inner and outer horizon coincides. In these limits it may be possible to get the eikonal limit using the WKB method following [43].

3.2 Massive scalar field perturbations

For massive scalar perturbation the Klein Gordon equation is given by

$$\frac{1}{\sqrt{-g}}\partial_\mu (\sqrt{-g}g^{\mu\nu}\partial_\nu\Phi) = \mu^2\Phi \quad (16)$$

where μ is scalar field mass. Similarly , we chosen the ansatz as in Eqn.10 and finally we have the Schrödinger-like equation and modified effective potential as

$$\begin{aligned} \frac{d^2U(r)}{dr_*^2} + (\omega^2 - V(r_*)) U(r) &= 0 \\ V(r) &= f(r) \left(\frac{l(l+1)}{r^2} + \frac{f'(r)}{r} + \mu^2 \right) \end{aligned}$$

where the tortoise coordinate r_* is related to r by $dr_* = \frac{dr}{f(r)}$.

In figure (7), we plot the effective potential $V(r)$ vs r for different scalar mass(μ). We have chosen the parameters $\Lambda = 0.007$, $M = 1$, $g = 0.5$ and $\ell = 3$. In figures (8-9), we have plotted

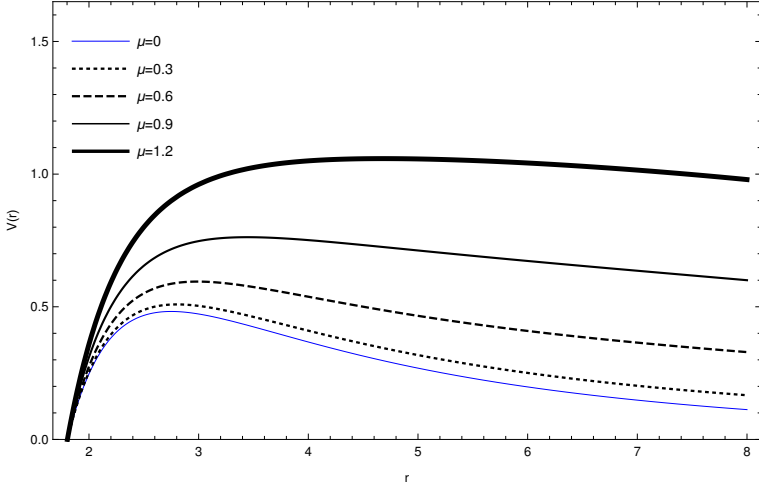


Figure 7: Variation of Potential $V(r)$ vs r for various masses(μ)

the variations of imaginary and real part of ω versus scalar field mass (μ) for different values of parameters Λ , M , g and l . We have plotted all the data obtained by 3rd, 4th, 5th and 6th order WKB calculations simultaneously to compare the accuracy between different orders. We

observed from the plots of both $\text{Im}(\omega)$ and $\text{Re}(\omega)$ that for low overtone number n , the accuracy between lower and higher order WKB is not much significant but for large n deviation is more. The magnitude of $\text{Im}(\omega)$ decreases with increasing scalar mass, on the contrary, the magnitude of $\text{Re}(\omega)$ increases with increasing field mass.

In table 2, we present the numerical values of QN frequencies with corresponding parameters. Since it is well known that WKB method is more accurate for $n < \ell$, we have tabulated the QNMs frequencies for $n < \ell$ only.

Scalar mass	Overtone number	3rd order WKB	6th order WKB
$\mu = 0$	$n = 0$	0.785191 -0.072860 i	0.785427 -0.072871 i
	$n = 1$	0.766662 -0.221907 i	0.767696 -0.221308 i
	$n = 2$	0.733146 -0.379935 i	0.731816 -0.376151 i
$\mu = 0.2$	$n = 0$	0.791386 -0.072173 i	0.791621 -0.072187 i
	$n = 1$	0.772648 -0.219660 i	0.773657 -0.219163 i
	$n = 2$	0.738382 -0.375726 i	0.737619 -0.372627 i
$\mu = 0.4$	$n = 0$	0.810314 -0.069906 i	0.810545 -0.069926 i
	$n = 1$	0.790571 -0.212544 i	0.791508 -0.212286 i
	$n = 2$	0.753616 -0.363179 i	0.754017 -0.361725 i
$\mu = 0.6$	$n = 0$	0.843078 -0.065359 i	0.843303 -0.065384 i
	$n = 1$	0.820174 -0.199327 i	0.821114 -0.199253 i
	$n = 2$	0.776829 -0.342952 i	0.778539 -0.342391 i
$\mu = 0.8$	$n = 0$	0.891821 -0.056961 i	0.892032 -0.057001 i
	$n = 1$	0.860107 -0.177635 i	0.861930 -0.177404 i
	$n = 2$	0.801532 -0.319314 i	0.811731 -0.313581 i

Table 2: Comparison between 3rd and 6th order WKB of QN frequencies due to massive scalar perturbation for $\Lambda = 0.001$, $g = 0.8$, $M = 1$ and multipole number $\ell = 3$.

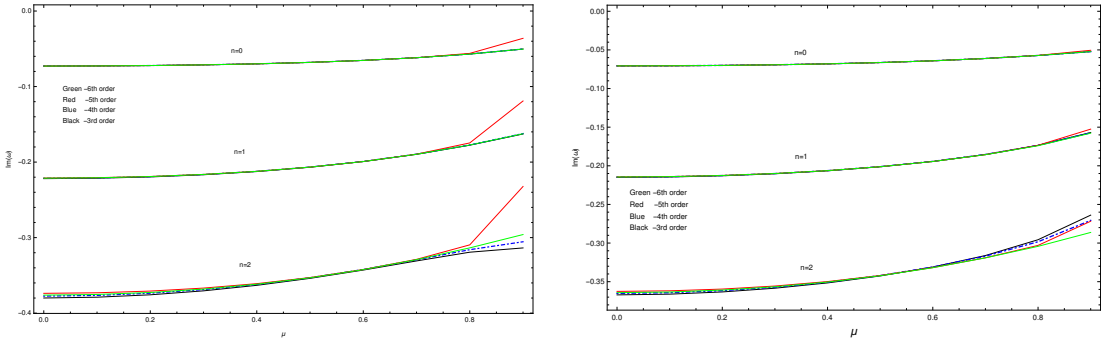


Figure 8: Variation of $\text{Im}(\omega)$ with scalar mass(μ) for $\Lambda = 0.001$ (left) and $\Lambda = 0.01$ (right). Here magnetic charge $g = 0.8$ and multipole number $\ell = 3$.

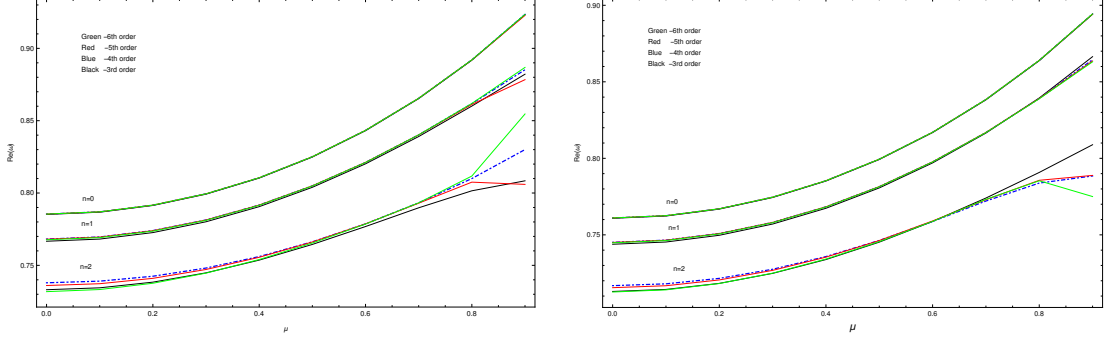


Figure 9: Variation of $\text{Im}(\omega)$ with scalar mass(μ) for $\Lambda = 0.001$ (left) and $\Lambda = 0.01$ (right). Here magnetic charge $g = 0.8$ and multipole number $\ell = 3$.

As in massless case, we plot in figures (10 & 11) the behaviour of QN frequencies with Λ and g for $n = 0$ and $\ell = 0, 1, 2$ respectively. $\text{Re}(\omega)$ increases with increasing value of magnetic charge g while magnitude $\text{Im}(\omega)$ decreases, on the other hand, figure 11 shows that $\text{Re}(\omega)$ decreases with an increase in cosmological constant(Λ) but $\text{Im}(\omega)$ increases with Λ in magnitude. With the scalar mass included, the oscillations decay faster with large Λ . The field oscillates better for large g in massive case.

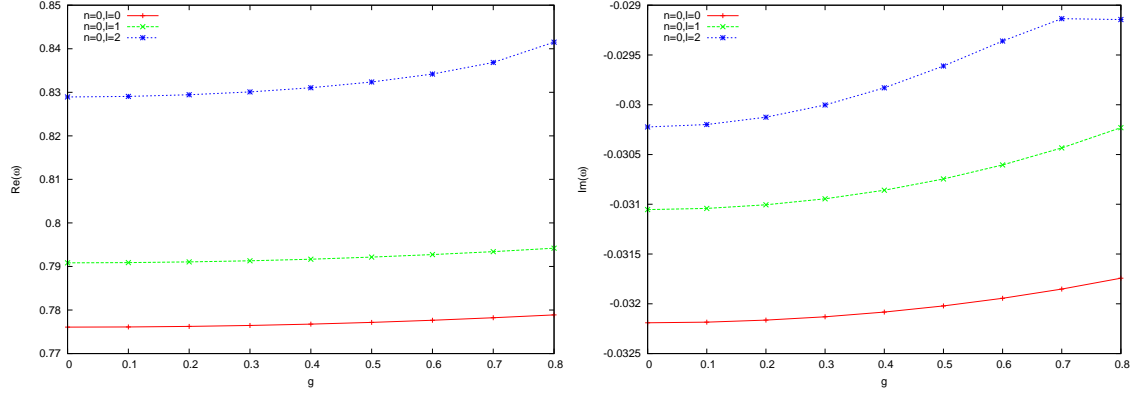


Figure 10: Variation of $\text{Re}(\omega)$ and $\text{Im}(\omega)$ with g , for $M = 1$, $\Lambda = 0.007$.

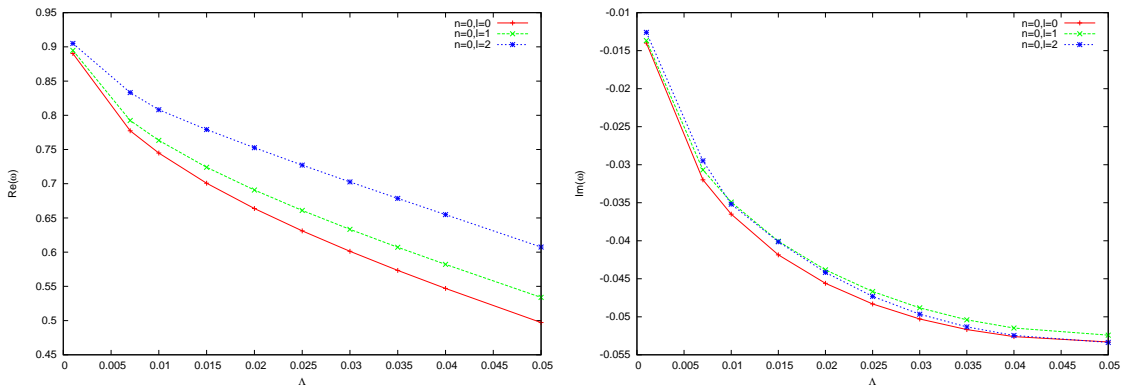


Figure 11: Variation of $\text{Re}(\omega)$ and $\text{Im}(\omega)$ with Λ , for $M = 1$, $g = 0.55$.

4 Dirac QNMs in BdS black hole

In this section we will extend our discussion to massless Dirac perturbations for BdS black holes. As in [44], by starting from dirac equation in spherically symmetric curved background, the Schrödinger-like equation we finally arrived at is given by

$$\left(-\frac{d}{dr_*^2} + V_1\right) G = E^2 G \quad (17)$$

$$\left(-\frac{d}{dr_*^2} + V_2\right) F = E^2 F \quad (18)$$

where r_* is the tortoise coordinate given by $f \frac{d}{dr} \equiv \frac{d}{dr_*}$, E is the energy. The effective potentials is given by

$$V_{1,2} = \pm \frac{dW}{dr_*} + W^2, \text{ where } W = \frac{\sqrt{f}}{r}(\ell + 1). \quad (19)$$

It is worth mentioning here that the potentials V_1 and V_2 corresponding to Dirac particles and anti-particles are supersymmetric to each other and derived from the same superpotential W . We will evaluate the quasinormal modes by solving equation [17] taking only V_1 as it is well known that both Dirac particles and anti-particles have the same quasi-normal spectra [48]. In figure (12), we showed the behaviour of the effective potential(V_1 only) for BdS black hole with spherical harmonic ℓ for parameters $M = 1, \Lambda = 0.007, g = 0.57$. We have computed the massless fermion

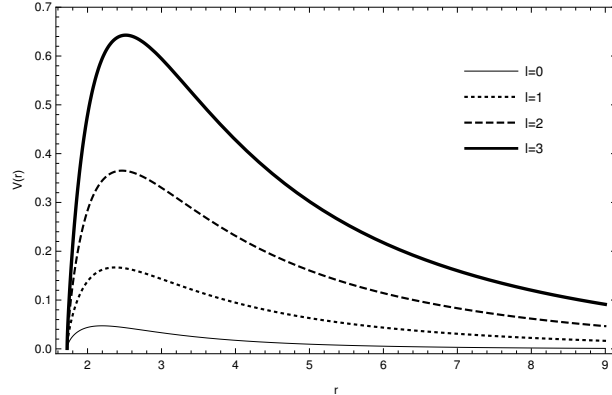


Figure 12: Variation of $V(r)$ vs r for different values of ℓ for the massless Dirac perturbations.

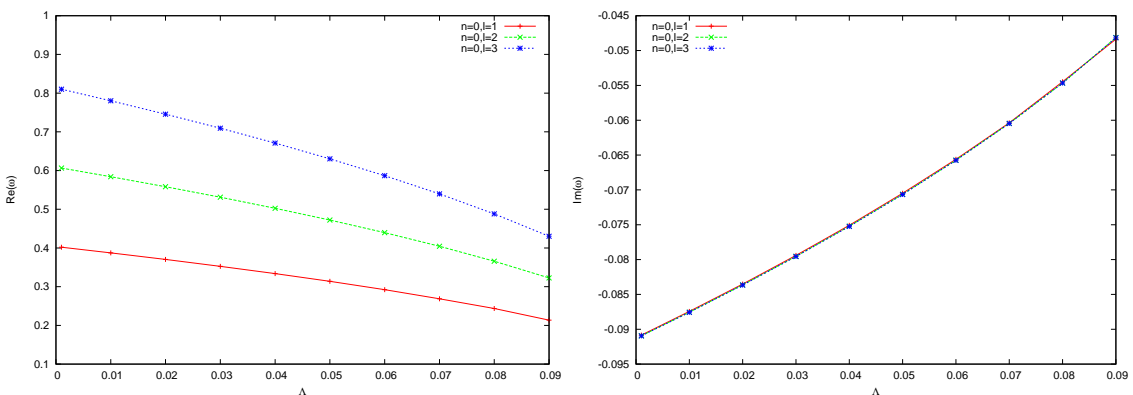


Figure 13: Variation of $\text{Re}(\omega)$ and $\text{Im}(\omega)$ vs Λ , for $M = 1, g = 0.55$.

QNMs semi-analytically using sixth order WKB method. The plots are shown in figure 13 , where we have shown the variation of real and imaginary part of ω with cosmological constant Λ and in figure 14 , the variation with magnetic charge g for different values of ℓ with fixed overtone number ($n = 0$) are shown. We can clearly see from the plots that $\text{Re}(\omega)$ slowly increases with an

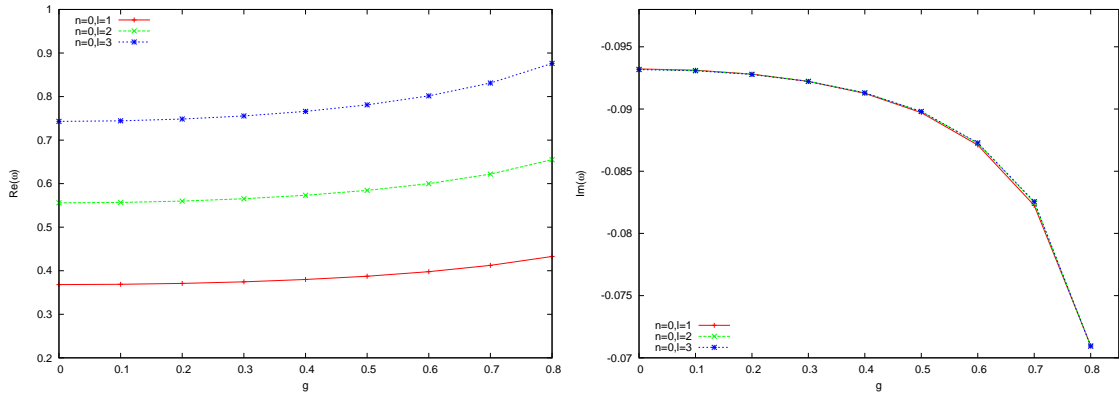


Figure 14: Variation of $\text{Re}(\omega)$ and $\text{Im}(\omega)$ vs g , for $M = 1$, $\Lambda = 0.007$.

increase in the magnetic charge g of the BdS black hole whereas it slowly decreases with increasing value of Λ . Whereas the behaviour of the imaginary part of the frequency reverses its role, i.e. as we increase the cosmological constant, the imaginary part increases, however it decreases if we increase the magnetic charge, keeping all other parameters fixed.

5 Summary and Conclusion

In this paper, we have discussed the massless and massive scalar field perturbations and the massless Fermionic perturbations for a regular BdS black hole. We have used sixth order WKB approximation method to calculate the QNMs frequencies. We studied how the frequencies vary as a function of the scalar field mass (μ), multipole number (ℓ) as well as with the parameters like the cosmological constant (Λ), black hole mass (M) and magnetic charge (g). We found that the QN frequencies decrease with an increase in black hole mass [42]. The plots of frequencies versus scalar mass show that $\text{Re } \omega$ increases with mass μ while $\text{Im } \omega$ decreases. The figures also suggested that if we plot the frequencies from low to higher overtones taking into account different WKB orders, we see that comparative accuracy is better for $\ell < n$. We found that $\text{Re } \omega$ decreases with an increase in cosmological constant Λ for scalar (both massless and massive) perturbations as well as with Dirac perturbations but $\text{Im } \omega$ decreases in massless and fermionics case however, increases for massive case when Λ is increased. We have also studied the behaviour of how the Q-factor for the massless scalar field varies with Λ and g .

For massive scalar perturbations, we see that mass μ enhances the field oscillations and decreases the damping for small Λ , unlike in the massless case where it is just the opposite. In all the three scenarios real frequency of oscillations $\text{Re } \omega$ increases steadily with magnetic charge (g) but the damping denoted by $\text{Im } \omega$ decreases.

For future directions, it would be interesting to study the time evolution of perturbations for this particular black hole. Apart from that, in [45], the authors have used the conformal properties of the spinor field to obtain the Dirac QNMs for a higher dimensional Schwarzschild-Tangherlini black hole. They have described these modes in the light of the so called split fermion models, where quarks and leptons exist on different branes in order to keep proton stability. Such split fermion theories also have massive fermions in the bulk and it will be interesting to study such massive Dirac perturbations in the context of higher dimensional generalization of the BdS black holes .

References

- [1] Kokkotas K D and Schmidt B G 1999 *Living Rev. Rel.* **2** 2
- [2] Nollert H-P 1999 *Class. Quantum Grav.* **16** R159
- [3] Berti E, Cardoso V and Starinets A O 2009 *Class.Quant.Grav.* **26** 163001
- [4] Konoplya R A and Zhidenko A 2011 *Rev.Mod.Phys.* **83** 793-836

- [5] Abbott B P et al. 2016 *Phys. Rev. Lett.* **116** 241102
- [6] Birmingham D, Sachs I and Solodukhin S N 2002 *Phys. Rev. Lett.* **88** 151301
- [7] Birmingham D, Sachs I and Solodukhin S N 2003 *Phys. Rev.* **D67** 104026
- [8] Horowitz G T and Hubeny V E 2000 *Phys. Rev.* **D62** 024027; Konoplya R A 2002 *Phys. Rev.* **D66** 044009
- [9] Cardoso V and Lemos J P S 2001 *Phys. Rev.* **D63** 124015
- [10] Hod S 1998 *Phys. Rev. Lett.* **81** 4293
- [11] Motl L and Neitzke A 2003 *Adv. Theor. Math. Phys.* **7** 307
- [12] Maggiore M 2008 *Phys. Rev. Lett.* **100** 141301
- [13] Perlmutter S *et al.* 1997 *Astrophys. J.* **483** 565
- [14] Riess A G et al. 1998 *Astron. J.* **116** 1009
- [15] Tegmark M et al. 2004 *Phys. Rev.* **D69** 103501
- [16] Strominger A 2001 *JHEP* **0110** 034
- [17] Strominger A 2001 *JHEP* **0111** 049
- [18] Abdalla E, Castello-Branco K H C and Lima-Santos A 2002 *Phys. Rev.* **D66** 104018
- [19] Konoplya R A 2003 *Phys. Rev.* **D68** 124017
- [20] Konoplya R A and Zhidenko A 2004 *JHEP* **06** 037;
- [21] Zhidenko A 2004 *Class. Quant. Grav.* **21** 273
- [22] Cardoso V and Lemos J P S 2003 *Phys. Rev.* **D67** 084020
- [23] Molina C 2003 *Phys. Rev.* **D68** 064007
- [24] Lopez-Ortega A 2006 *Gen. Rel. Grav.* **38** 1565
- [25] Lopez-Ortega A 2006 *Gen. Rel. Grav.* **38** 743
- [26] Lopez-Ortega A 2007 *Gen. Rel. Grav.* **39** 1011
- [27] Lopez-Ortega A 2008 *Gen. Rel. Grav.* **40** 1379
- [28] Smirnov A A 2005 *Class. Quant. Grav.* **22** 4021
- [29] Bardeen J M 1968 *Proceedings of GR5 (Tbilisi)* 174
- [30] Ayón-Beato E and García A 2000 *Phys. Lett.* **B493** 149
- [31] Ayón-Beato and García A 1998 *Phys. Rev. Lett.* **80** 5056
- [32] Bronnikov K A 2001 *Phys. Rev.* **D63** 044005
- [33] Hayward S A 2006 *Phys. Rev. Lett.* **96** 031103
- [34] Dymnikova I 2004 *Class. Quant. Grav.* **21** 4417
- [35] Bronnikov K A and Fabris J A 2006 *Phys. Rev. Lett.* **96** 251101
- [36] Moreno C and Sarbach O 2003 *Phys. Rev.* **D67** 024028
- [37] Flachi A and Lemos J 2013 *Phys. Rev.* **D87** 024034
- [38] Fernando S and Correa J 2012 *Phys. Rev.* **D86** 64039
- [39] Man J and Cheng H 2014 *Gen. Rel. Grav.* **46** 1559

- [40] Zhou S, Chen J and Wang Y 2012 *Int. Jour. Mod. Phys. D* **21** 1250077
- [41] Fernando S, arXiv: 1611.05337 [gr-qc]
- [42] Fernando S , Correa Juan 2012 *Phys. Rev* **D86** 064039
- [43] Cardoso V, Berti E, Witek H, Zanchin V T 2009 *Phys.Rev.* **D79** 064016
- [44] D. R. Brill and J. A. Wheeler, *Rev. Mod. Phys.* **29**, 465 (1957).
- [45] Cho H T, Cornell A S, Doukas J and Naylor W 2007 *Phys. Rev* **D75** 104005
- [46] Iyer S and Will C M 1987 *Phys. Rev* **D35** 3621
- [47] Konoplya R A 2003 *Phys. Rev.* **D68** 024018
- [48] Jing J L 2004 *Phys. Rev* **D69** 084009